Supplementary Information

Single-step solid-state synthesis and characterization of $Li_4Ti_{5-x}Fe_xO_{12-y}$ ($0 \leq x \leq 0.1$) as an anode for lithium-ion batteries

Guijun Yang and Soo-Jin Park*

[*] Corresponding author: S. J. Park, Ph.D.
Department of Chemistry and Chemistry Engineering, Inha University, 253, Nam-gu, Incheon 402-751, Korea (south),
Tel.: +82-32-860-8438, Fax: +82-32-860-8438
E-mail: sjpark@inha.ac.kr.

2.3. Characterization of the synthesized materials

To evaluate the characteristic of the obtained samples, SDTQ600 thermogravimetric analysis/differential scanning calorimetry (TGA-DSC) system was used to identify the phase transition temperature in N_2 atmosphere with a flow rate of 30 mL min^{-1} from 25 °C to 900 °C at a heating rate of 3°C min^{-1}. X-ray diffraction (XRD, Bruker D2 PHASER) was employed to analyze the composition of the samples. Scanning electron microscopy (SEM, Model SU8010, Hitachi Co., Ltd.) was used to characterize the structure and morphology, Energy dispersive X-ray (EDX) measurements were conducted using the EDAX system attached to the same microscope. The XPS spectra were obtained with ESCALAB250 XPS (Thermo Fisher Scientific, USA) at 2×10^{-9} mbar. Al Ka (1486.6 eV) was used as the X-ray source at 15 keV of anode voltage, all binding energies were referenced to the C1s peak (284.8 eV) arising from adventitious carbon.

2.4. Electrochemical measurement

Coin cells (CR2032) were assembled to test the electrochemical performance of the obtained samples. The working electrode was prepared by coating a slurry of active material (80 wt. %), carbon black (electronic conductive additive, 10 wt. %), and poly vinylidene fluoride (PVDF, binder, 10 wt. %) in N-methyl pyrrolidone (NMP) solution onto a copper foil. The obtained electrodes were then dried at 110 °C overnight under a vacuum. The half cells were assembled in an Ar-flled glovebox. Celgard 2400 and lithium was used as separator and counter electrode, respectively. The galvanostatic charge/discharge characteristics of cells were performed in a voltage range of 0-3.0V (vs. Li/Li^+) at various rates using LAND CT2001 battery tester. The specific capacity was calculated based on the active mass of the electrode. Electrochemical impedance

spectroscopy (EIS) measurements were performed on a Zennium/IM6 electrochemical workstation (Zahner, Germany) with an oscillating voltage of 5 mV over frequency ranging from 10^{-2} to 10^{5} Hz. Cyclic voltammetry (CV) were obtained using the same workstation as EIS measurements in the voltage range of 0-3.0 V (vs. Li/Li^{+}) at different scan rates.

2.5. Theoretical method and structure model

First-principles calculations were performed by the first-principles total-energy pseudopotential method (density function theory, DFT) implemented in CASTEP (Cambridge Serial Total Energy Package). The exchange-correlation function was constructed by the generalized gradient approximation (GGA) with the Perdew–Burke–Ernzerhof (PBE). The convergence test of total energy with respect to k-point sampling has been carefully examined. The total energies are converged better than 10^{-5} eV. All calculations were performed using the Monkhorst Pack k-point grid. For all the DOS calculations, the Gaussian smearing method is used and the broadening width is 0.05 eV. Since the LTO system is non-magnetic, spin polarization is ignored in the calculation.

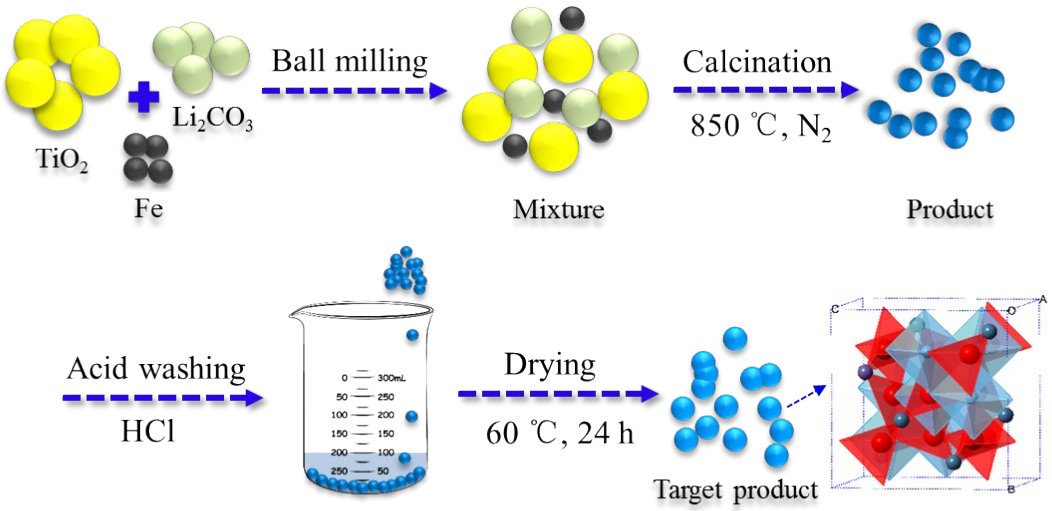

Scheme 1. Schematic of the preparation of target product $Li_4Ti_{5-x}Fe_xO_{12}$.

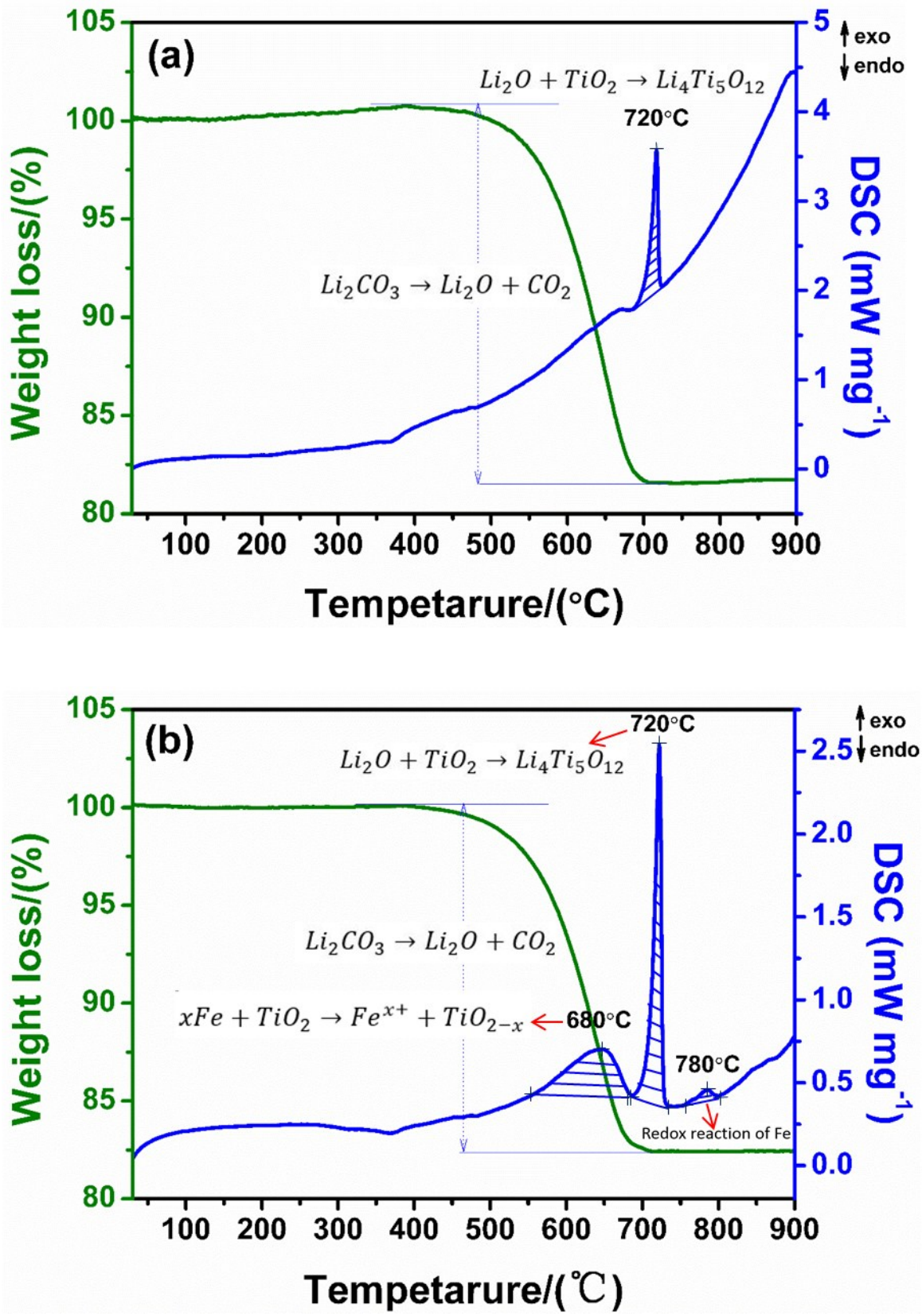

Figure S1. TGA-DSC measurement of raw material mixture of a stoichiometric ratio of (a) pure LTO (Li_2CO_3, TiO_2) and (b) $Li_4Ti_{5-x}Fe_xO_{12}$ (Li_2CO_3, TiO_2 and Fe).

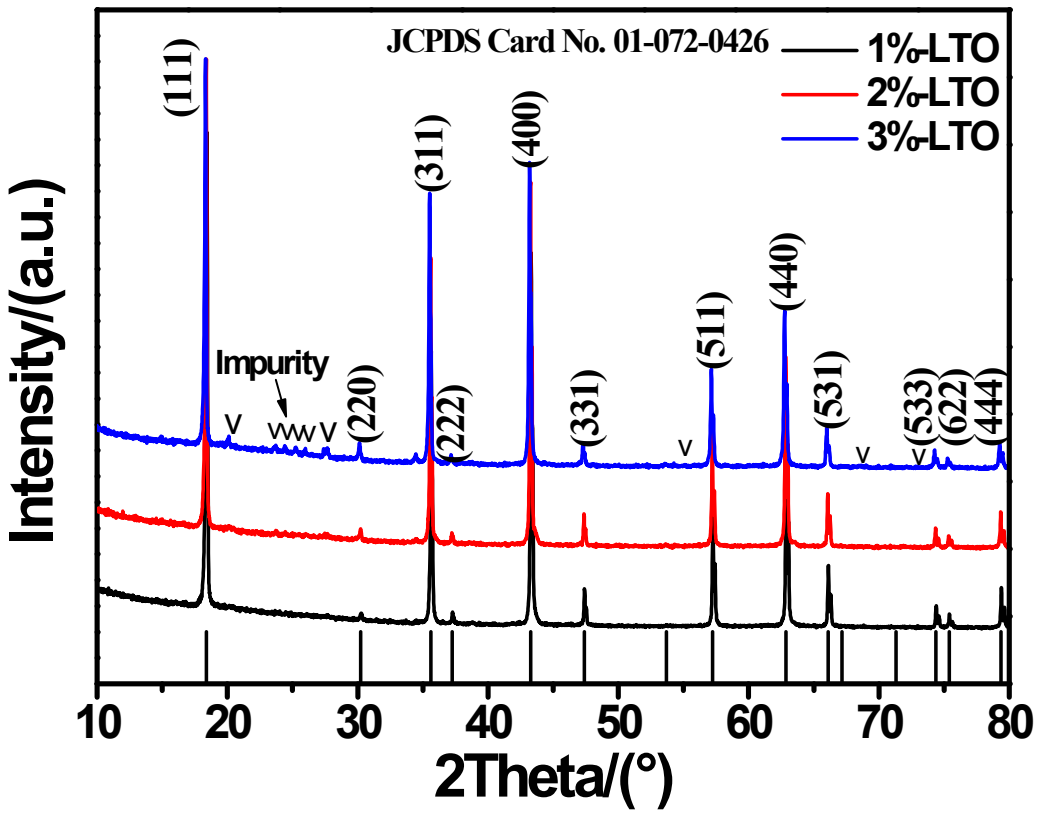

Figure S2. TGA-DSC measurement of raw material mixture of a stoichiometric ratio of (a) pure LTO (Li_2CO_3, TiO_2) and (b) $Li_4Ti_{5-x}Fe_xO_{12}$ (Li_2CO_3, TiO_2 and Fe).

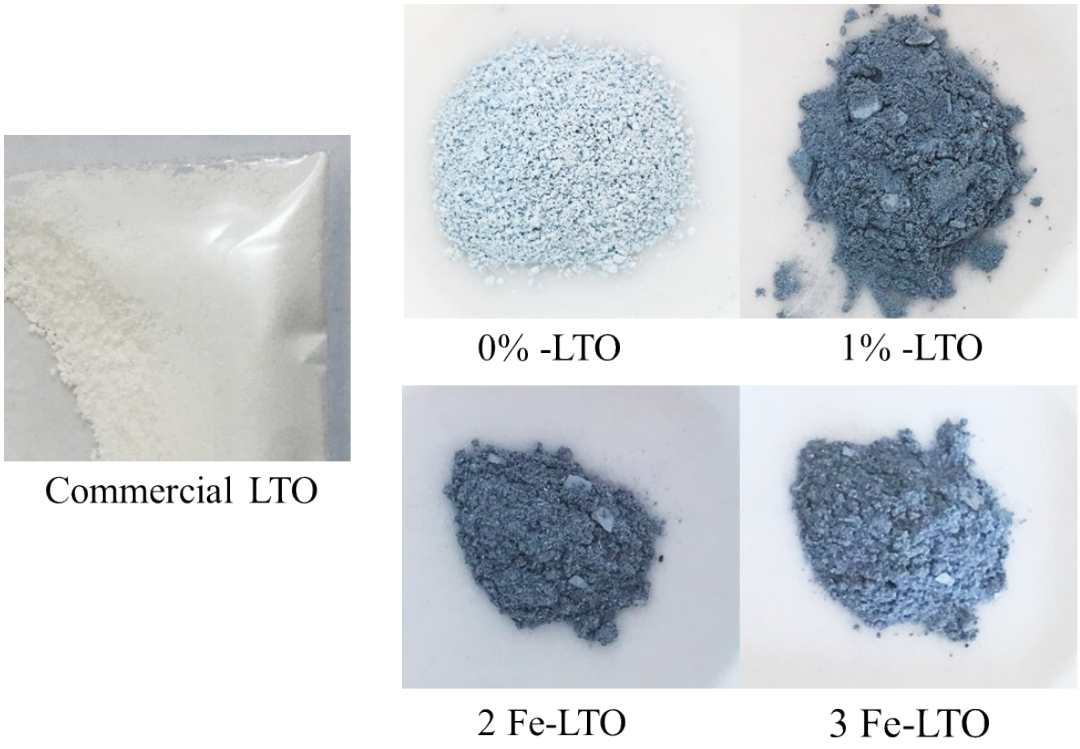

Figure S3. The electronic photograph of commercial LTO and $Li_4Ti_{5-x}Fe_xO_{12}$ with different content of Fe (0%-LTO, 1%-LTO, 2%-LTO and 3%-LTO).

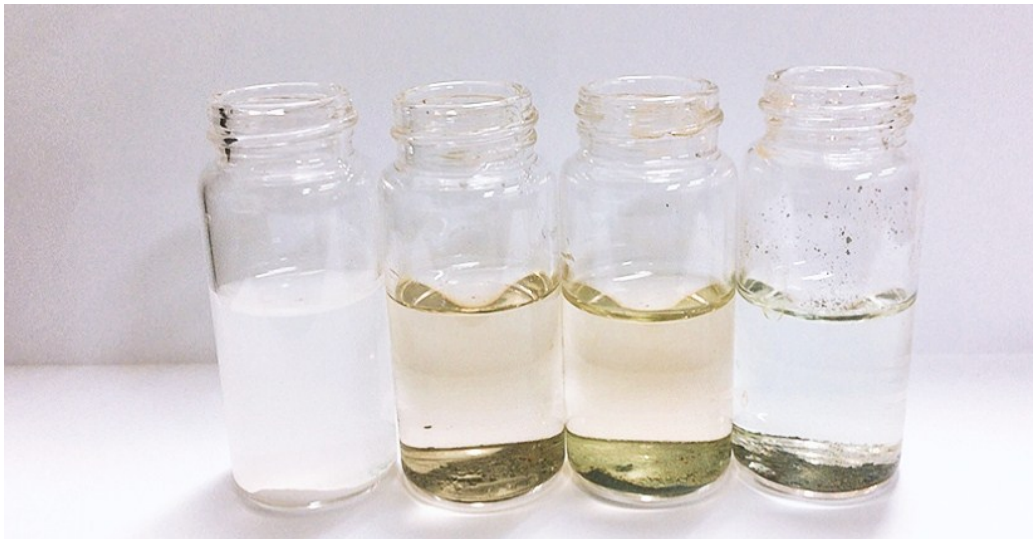

Figure S4. The electronic photograph of the aqueous solution obtained after acid treatment of the $Li_4Ti_{5-x}Fe_xO_{12}$ with different Fe contents (0%-LTO, 1%-LTO, 2%-LTO, and 3%-LTO).

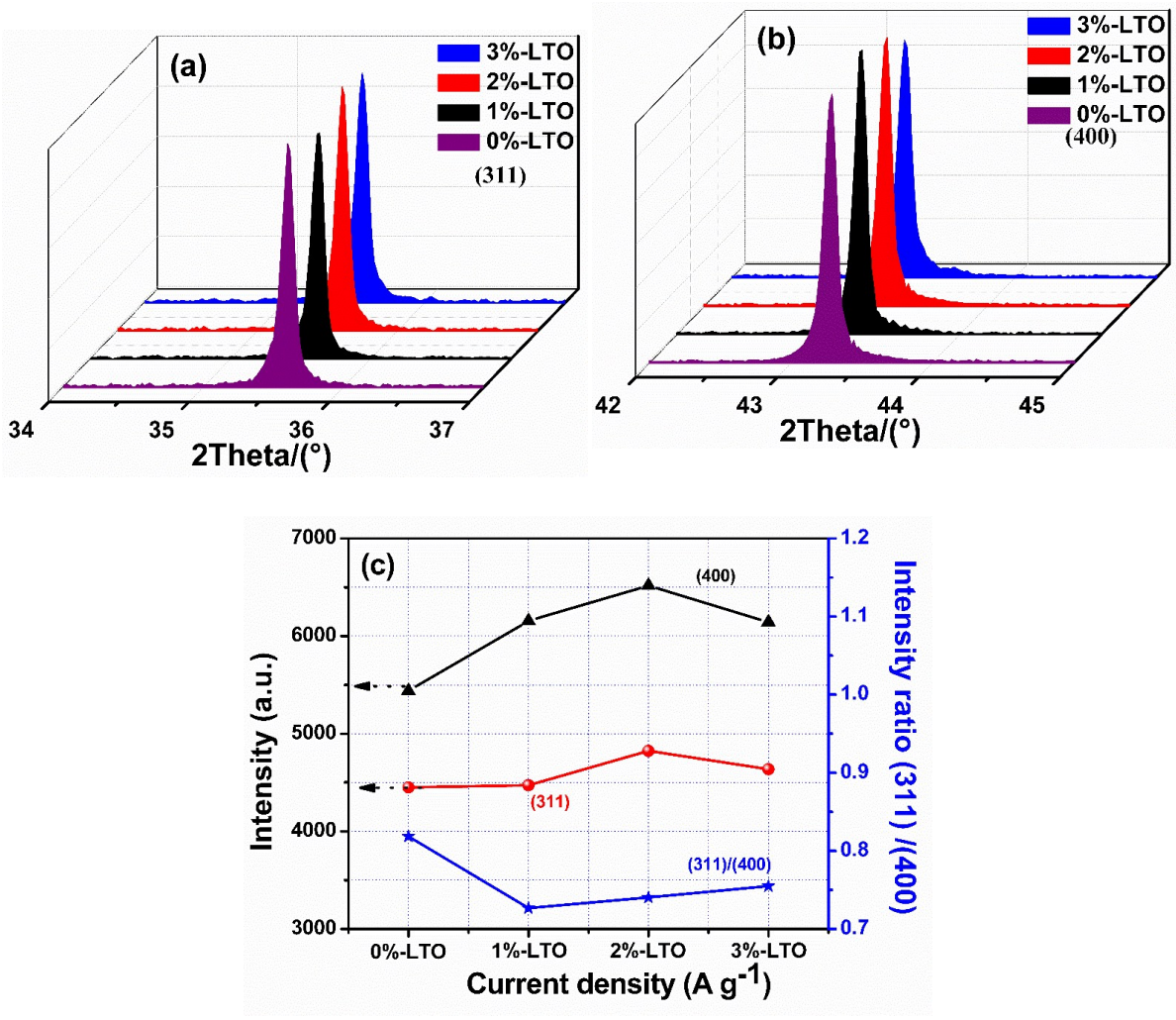

Figure S5. Magnified views of (a) (311), (b) (400) and of (c) intensity ratio (311)/(400) of $Li_4Ti_{5-x}Fe_xO_{12}$ with different Fe contents (0%-LTO, 1%-LTO, 2%-LTO, and 3%-LTO).

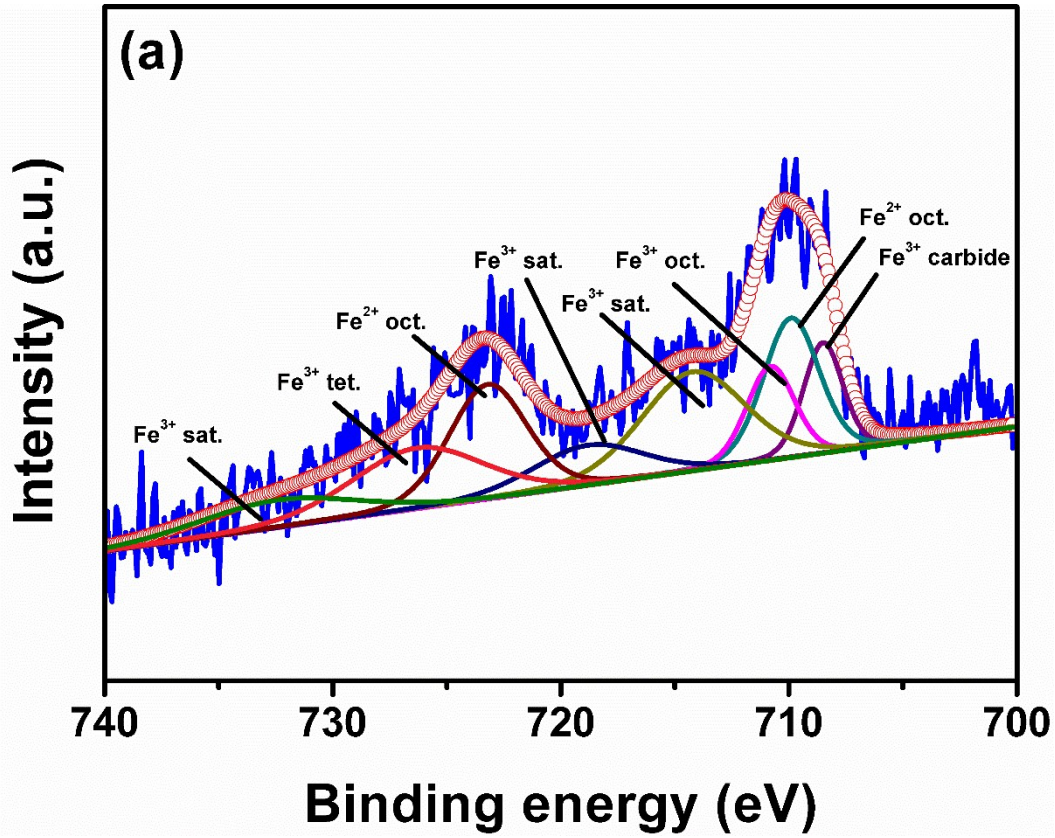
(a)
Intensity (a.u.)
Fe3+ sat.
Fe3+ tet.
Fe2+ oct.
Fe3+ sat.
Fe3+ oct.
Fe3+ sat.
Fe2+ oct.
Fe3+ carbide
740
730
720
710
700
Binding energy (eV)

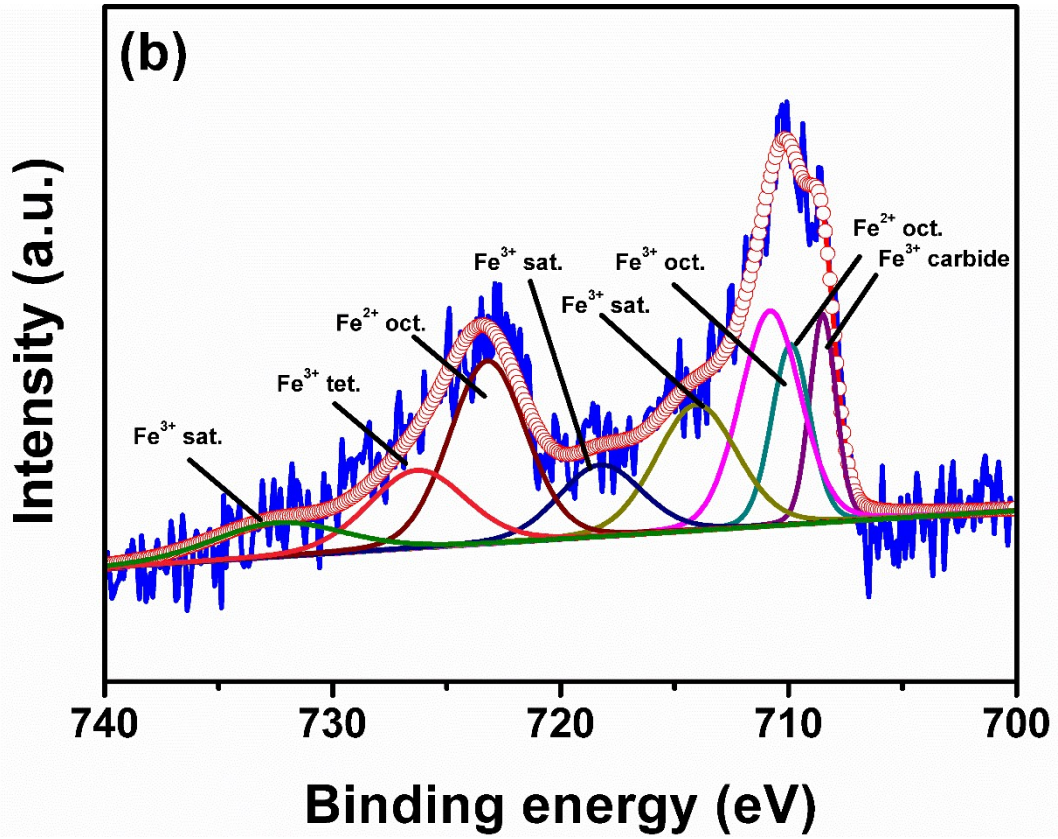
(b)
Intensity (a.u.)
Fe3+ sat.
Fe3+ tet.
Fe2+ oct.
Fe3+ sat.
Fe3+ oct.
Fe3+ sat.
Fe2+ oct.
Fe3+ carbide
740
730
720
710
700
Binding energy (eV)

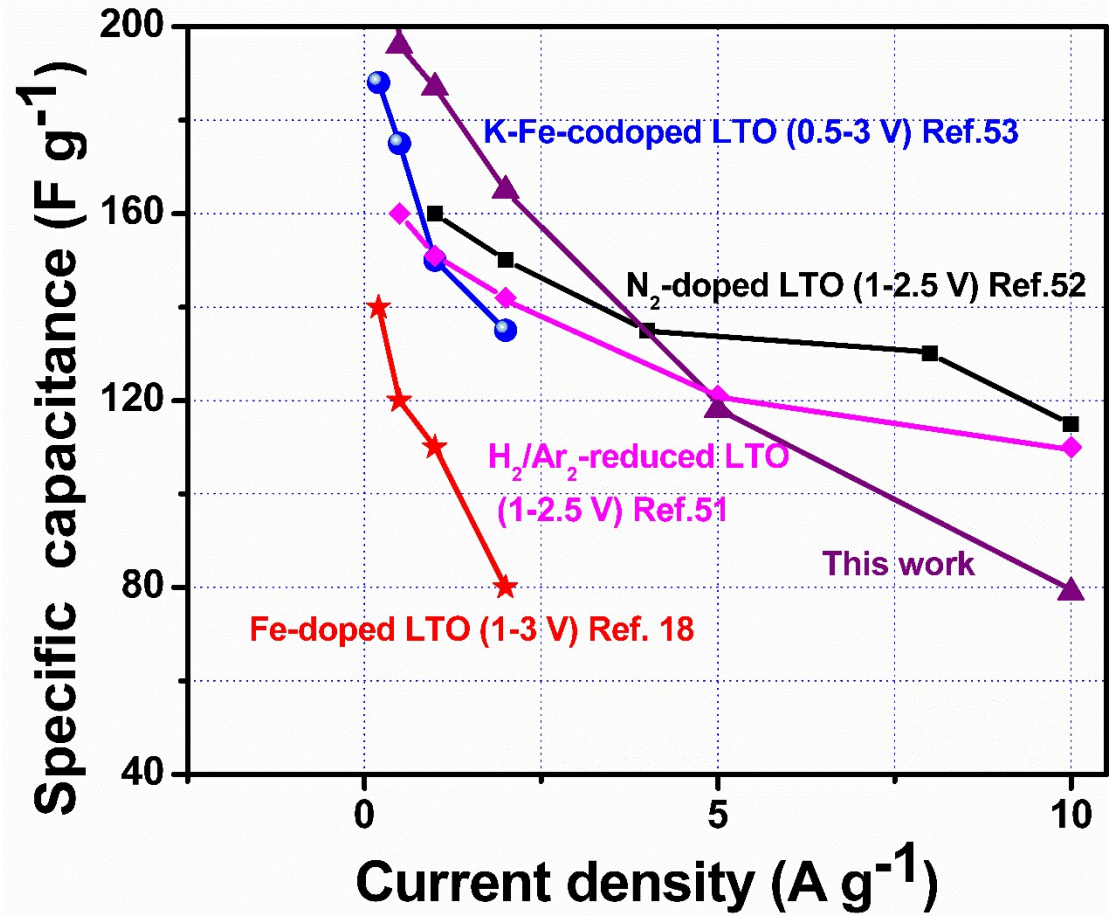

Figure S7. The comparison of rate capability of 2%-LTO with other LTO-based high-rate electrodes in recently reported works. The capacities were estimated based on their results of rate performance.

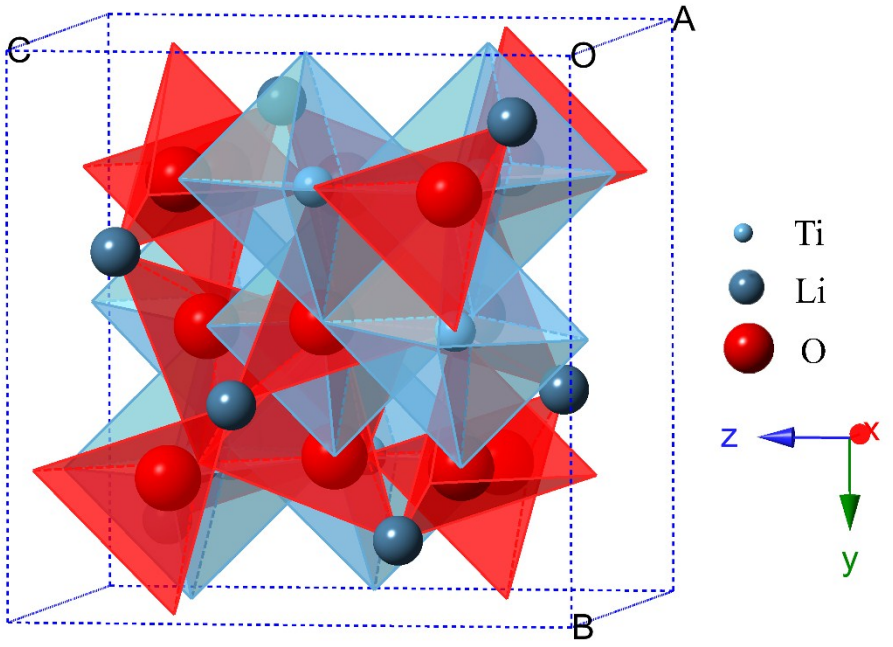
C
A
O
B
Ti
Li
O
z
x
y

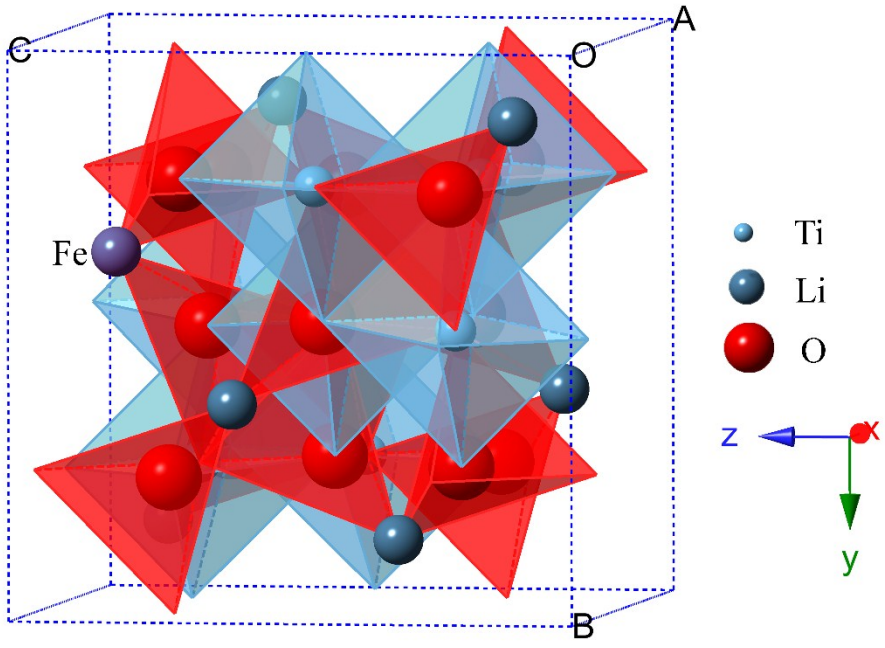
C
A
O
Fe
B
Ti
Li
O
z
x
y

Figure S8. The cubic crystalline structure of $Li_4Ti_5O_{12}$ and Fe-doped $Li_4Ti_5O_{12}$**.**

Table 1. The binding energy of the Fe 2p.

Name	Position (eV)
$Fe^{carbide}$ $2p_{3/2}$	708.5
Fe^{2+} oct $2p_{3/2}$	709.9
Fe^{3+} oct $2p_{3/2}$	710.8
Fe^{3+} sat $2p_{3/2}$	714.2
Fe^{3+} sat $2p_{3/2}$	718.8
Fe^{2+} oct $2p_{1/2}$	723.2
Fe^{3+} tet $2p_{1/2}$	726.3
Fe^{3+} sat $2p_{1/2}$	732.4

Note: oct, octahedral; tet, tetrahedral; sat, satellite

Table 2. The Fe atomic ratio of $Li_4Ti_{5-x}Fe_xO_{12}$ with different contents of Fe (0%-LTO, 1%-LTO, 2%-LTO, and 3%-LTO).

Name	Atomic % (XPS)
0%-LTO	0
1%-LTO	0.76
2%-LTO	1.16
3%-LTO	1.61